

This item is the archived peer-reviewed author-version of:

Goodenough-Kanamori-Anderson high-temperature ferromagnetism in tetragonal transition-metal xenes

**Reference:**

Yorulmaz Ugur, Šabani Denis, Sevik Cem, Milošević Milorad.- Goodenough-Kanamori-Anderson high-temperature ferromagnetism in tetragonal transition-metal xenes  
2D materials - ISSN 2053-1583 - 11:3(2024), 035013  
Full text (Publisher's DOI): <https://doi.org/10.1088/2053-1583/AD3E08>  
To cite this reference: <https://hdl.handle.net/10067/2054640151162165141>

# Goodenough-Kanamori-Anderson high-temperature ferromagnetism in tetragonal transition-metal xenes

U. Yorulmaz<sup>†</sup>

Department of Physics, Eskisehir Osmangazi University, Eskisehir, Turkiye  
Department of Physics & NANOLab Center of Excellence, University of Antwerp,  
Groenenborgerlaan 171, B-2020 Antwerp, Belgium

D. Šabani<sup>†</sup>

Department of Physics & NANOLab Center of Excellence, University of Antwerp,  
Groenenborgerlaan 171, B-2020 Antwerp, Belgium

C. Sevik

Department of Mechanical Engineering, Eskisehir Technical University, Eskisehir,  
Turkiye  
Department of Physics & NANOLab Center of Excellence, University of Antwerp,  
Groenenborgerlaan 171, B-2020 Antwerp, Belgium

M. V. Milošević<sup>‡</sup>

Department of Physics & NANOLab Center of Excellence, University of Antwerp,  
Groenenborgerlaan 171, B-2020 Antwerp, Belgium

**Abstract.** Seminal Goodenough-Kanamori-Anderson (GKA) rules provide the inceptive understanding of the superexchange interaction of two magnetic metal ions bridged with an anion, and suggest fostered ferromagnetic interaction for orthogonal bridging bonds. However, there are no examples of two-dimensional (2D) materials with structure that optimizes the GKA arguments towards enhanced ferromagnetism and its critical temperature. Here we reveal that an ideally planar GKA ferromagnetism is indeed stable in selected tetragonal transition-metal xenes (tTMXs), with Curie temperature above 300 K found in CrC and MnC. We provide the general orbitally-resolved analysis of magnetic interactions that supports the claims and sheds light at the mechanisms dominating the magnetic exchange process in these structures. Furthermore, we propose the set of three GKA-like rules that will guarantee room temperature ferromagnetism (FM). With recent advent of epitaxially-grown tetragonal 2D materials, our findings earmark tTMXs for facilitated spintronic and magnonic applications, or as a desirable magnetic constituent of functional 2D heterostructures.

<sup>†</sup> These authors contibuted equally to this work.

<sup>‡</sup> *Email: milorad.milosevic@uantwerpen.be*

## 1. Introduction

The experimental discovery of the premiere magnetic two-dimensional materials (M2DMs) - CrI<sub>3</sub> [1] and CrGeTe<sub>3</sub> [2, 3] - opened the floodgates to many emergent 2D materials of this class. Numerous theoretical [4, 5, 6, 7] and experimental studies [8, 9, 10, 11] followed, explaining the origins and possible manipulations of the long-range magnetic order in the monolayer limit. It is needless to emphasize that intrinsically room-temperature M2DMs would be highly beneficial for applications in sensing, spintronics, and otherwise, and bear promise towards high tunability by diverse mechanical, chemical, and electronic means. However, it quickly became clear that critical temperatures ( $T_c$ ) for magnetic order to vanish are by rule always smaller in 2D materials compared to their bulk counterparts [1, 12, 13]. Namely, in order to host sizable regions with magnetic order (and circumvent limitations imposed by the Mermin-Wagner theorem [14]), M2DMs require anisotropy in magnetic exchange. That needed anisotropy is known to originate from the spin-orbit coupling (SOC), which is in general much weaker compared to e.g. Coulomb attraction or repulsion of charged particles, hence attains very low magnitudes (of typically 0.01-0.1 meV). Another reason for  $T_c$  to decrease as one thins the magnetic material from bulk to a monolayer stems from the correspondingly diminishing magnetic exchange along the third, out-of-plane direction. One may therefore expect that magnetic order in 2D materials is strictly limited to the very low  $T_c$ , but that is not necessarily the case. For example, Fe<sub>3</sub>GeTe<sub>2</sub> hosts the ferromagnetic (FM) order up to 130 K in the monolayer (ML) limit [15]. In addition, the FM order and  $T_c$  of 213 K were measured in few-layer thick 1T-CrTe<sub>2</sub> [16], with the unusual trend that  $T_c$  increases as one goes from bulk to few-layers. Furthermore, in a few-layer FePS<sub>3</sub>, the antiferromagnetic (AFM) order was observed up to the  $T_c$  of 120 K [17]. Finally, FM order was measured even at room temperature in thicker films ( $\approx 10$  nm, see e.g. [18, 19]), but also in monolayer MnSe<sub>x</sub> [20, 21], VSe<sub>2</sub> [11, 22], and Cr<sub>3</sub>Te<sub>4</sub> [23]. The latter samples were deposited epitaxially, which in general involves structural defects [22] and strong interfacial effects with the substrate [22, 23] into the origins of the observed robust magnetic interactions, which complicates theoretical interpretations. Otherwise, the isotropic magnetic interactions in crystalline monolayers are relatively straightforward to extract theoretically in all available first-principles codes. Such studies, on predominantly *in silico* created 2D materials, have yielded many predictions of high- or even room-temperature intrinsic magnetism [24, 25, 26, 27, 28, 21]. However, those predictions typically failed to quantify the underlying microscopic mechanisms for such a large predicted magnetic exchange.

In this paper we therefore take a step back, and explore the route towards room-temperature 2D ferromagnetism starting from the well-established set of Goodenough-Kanamori-Anderson (GKA) empirical theoretical rules from the late 1950s [29, 30, 31, 32]. We accordingly aim at monolayers with 90° between the nearest magnetic atoms (A) connected by a ligand (X), thus ideally a *Lieb-lattice material* of A<sub>2</sub>X type. However, a magnetic 2D material of such specific planar structure has not been reported to

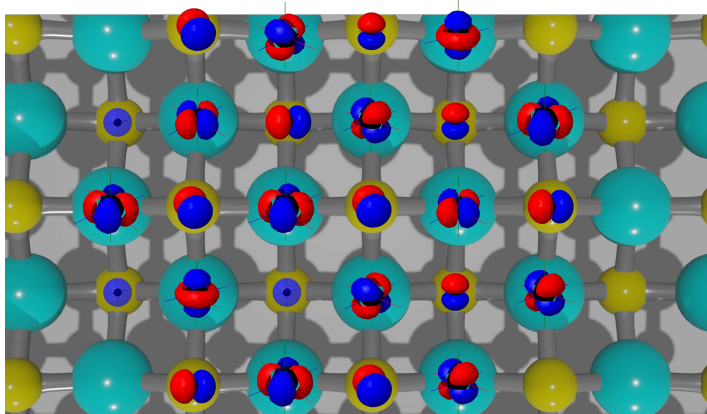


Figure 1: **Crystal structure of a monolayer *t*TMX.** TM (cyan) atoms are sketched with one *d* orbital, and X (yellow) atoms with one *p* orbital, since these orbitals and their hybridization are essential for magnetic interactions in this system.

date, although some Lieb-lattice 2D materials have been considered computationally for other purposes (see e.g. Ref. [33]). As a best available choice, for not only geometry but also sizable SOC, we instead focus on the family of tetragonal transition-metal xenes (*t*TMXs; see Fig. 1), seeking a square-lattice planar material among them - still with  $90^\circ$  TM-X-TM nearest-neighbor bonds. Such square-lattice planar materials are not yet present in monolayer form, however few nanometers thick (roughly 5-30 nm) layered structures from this family are easily synthesized.[34] Furthermore, in mentioned work, Kang *et al.* grew two distinctive phases of FeTe - low-temperature-grown tetragonal phase that showed AFM order and high-temperature-grown hexagonal phase that showed FM order - by controlling the temperature of crystal formation. Using advanced methodology on top of the standard first-principles approaches based on Density Functional Theory (DFT), we computationally validate the structural stability and strong intrinsic magnetic interactions in these materials, detail the microscopic (orbital-resolved) origin of enhanced magnetic exchange, and identify CrC and MnC as premiere square-lattice monolayer ferromagnets with a particularly high  $T_c$ .

## 2. Results

We commence our analysis with a computationally crude throughput screening of dynamical stability and magnetic interactions in *t*TMXs (where TM = V, Cr, Mn, Fe, Co, Ni, Cu, Zn, and X = C, N, O, S, Se, Te). For each stable material we perform total energy mapping between the density functional theory corrected with on-site Coulomb repulsion (DFT+ $U$ ) and the Heisenberg model Hamiltonian, for six particular magnetic orders - namely FM and AFM orders along three Cartesian directions (see Appendix B in † Supplementary Information), in order to extract the governing magnetic interactions in the system. For the sake of screening, Hubbard parameter  $U$  in the calculations is taken from the online database, based on bulk oxides of transition metals [35]. In order to

decrease computational cost, we consider only the first nearest-neighbor (NN) magnetic interactions and the single-ion anisotropy (SIA) in the Heisenberg Hamiltonian.

The considered primitive unit cell of these materials consists of two TM, and two X atoms - such that each TM atom has four X atoms as the nearest neighbors, and vice versa (see Fig. 1), where one can apply symmetry rules for the exchange matrix (see Appendix A in † Supplementary Information) and SIA (cf. Ref. [36]). In Fig. 1 each TM atom is sketched with one *d* orbital, and each X atom with one *p* orbital, since these atomic orbitals, and their mutual hybridization, are essential for the interactions between magnetic moments on TM atoms. Though the positions of the atoms in the structure are uniquely determined with respect to the in-plane primitive lattice vectors due to the symmetry of tetragonal structures, both atomic species are allowed to relax out-of-plane (along  $\vec{a}_3 \equiv z$  axis).

Table 1: **Magnetic properties of the stable monolayer tTMX structures.** FM, AFM, and NM stand for ferromagnetic, antiferromagnetic, and non-magnetic order, respectively.  $J^{xx}$  and  $J^{yy}$  mark in-plane, and  $J^{zz}$  out-of-plane exchange interactions. Out-of-plane exchange anisotropy  $\Delta$  stands for the difference  $J^{xx}-J^{zz}$ .  $A_{ii}^{zz}$  is the single-ion anisotropy (SIA). If signs of SIA and exchange interactions are the same, SIA favors out-of-plane anisotropy, otherwise the in-plane one.  $J^{xx}$ ,  $J^{yy}$ ,  $J^{zz}$ ,  $\Delta$ , and  $A_{ii}^{zz}$  are all given in meV.  $T_c$  stands for the critical temperature of the magnetic order, Curie for FM and Néel temperature for AFM monolayers.

	Magnetic order	$J^{xx}=J^{yy}$	$J^{zz}$	$\Delta$	$A_{ii}^{zz}$	$T_c(\text{K})$
CrC	FM	-52.68	-52.66	0.03	-0.35	515.6
MnC	FM	-105.98	-106.01	-0.03	-0.67	1065.8
VN	FM	-3.73	-10.54	-6.81	-13.94	152.4
CoN	FM	-12.57	-12.94	-0.38	1.28	132.2
NiTe	FM	-7.42	-5.15	2.27	4.53	31.2
FeC	AFM	53.00	53.28	0.28	0.21	5.3
FeO	AFM	5.47	5.46	-0.01	2.48	20.1
MnS	AFM	55.07	55.95	0.88	1.69	15.2
FeS	AFM	16.13	16.38	0.25	-0.56	5.7
MnSe	AFM	50.66	50.65	-0.01	-0.20	10.3
FeSe	AFM	15.30	15.24	-0.06	-1.20	5.8
FeTe	AFM	31.80	-28.89	-60.69	119.63	35.6
CuC	NM	-	-	-	-	-
NiN	NM	-	-	-	-	-
CuN	NM	-	-	-	-	-
NiS	NM	-	-	-	-	-
CuS	NM	-	-	-	-	-
ZnS	NM	-	-	-	-	-
CuSe	NM	-	-	-	-	-
ZnSe	NM	-	-	-	-	-
ZnTe	NM	-	-	-	-	-

Our throughput computational screening revealed that out of a 48 materials in total, only the 21 listed in Table 1 possess dynamical stability. Out of those 21, we identified five materials with FM order as lowest in energy (out of six possibilities considered), seven materials with AFM order as the lowest-energy one, and nine materials not exhibiting magnetic order, i.e. with magnetic moments on individual atoms below  $0.5\mu_B$  in every of the six considered magnetic configurations, and the configuration with magnetic moments exactly 0 as lowest in energy. Out of five FM materials, two of them appear to have completely flat, square lattice when on-site Coulomb repulsion between electrons ( $U$ ) is properly included - CrC and MnC. Such a structure ensures that the first-nearest-neighbor TM-X-TM bond comprises 90 degrees angle, and second-nearest-neighbor 180 degrees angle, making these structures optimal - according to GKA rules - for “maximization” of magnetic exchange in the system. This fact served as motivation to thoroughly analyze the structural, electronic, and magnetic properties of these two materials, and discuss the subtle interplay of these properties that optimizes the ferromagnetic order.

The first important finding concerns the structure. Namely, as indicated above, the relative atomic arrangement along the  $z$  axis strongly depends on the on-site Coulomb repulsion ( $U$ ) between electrons on TM atoms. In Fig. 2(a, b, e and f), we present the relaxed structures for CrC and MnC with no  $U$  included, and for the  $U$  value calculated self-consistently - using the linear response theory as introduced by Timorov *et al.* [37]. The latter  $U$  value is found as 3.29 eV for CrC, and 3.81 eV for MnC. In case of  $U=0$ , the structure buckles, and two X atoms relax above and below the plane of TM atoms. Furthermore, the X atoms create the tetrahedral structure around each TM atom. On the contrary, when using a realistic value for  $U$ , both CrC and MnC exhibit an ideally planar structure, i.e. a 2D square lattice as desired in the GKA argumentation towards the enhanced ferromagnetic order. For certainty, we tested the dynamical stability of both these planar structures - and the phonon dispersions shown in Fig. 2(c, d, g and h) exhibited no imaginary phonon frequencies.

After determining the on-site Coulomb repulsion and the planar structural stability, we move on to the magnetic properties of CrC and MnC. The necessary, yet insufficient condition for long-range magnetism is the non-zero magnetic moment per unit space. The TM atoms are expected to provide the latter, due to the localized unpaired electrons in their  $3d$  shell, each electron carrying spin  $\frac{1}{2}$ , and spin magnetic moment of  $1 \mu_B$ . In most of the structures based on TMs, the contribution of the orbital magnetic moment is negligible compared to the spin magnetic moment, due to the quenching of orbital momentum, hence the magnetic moment can be assumed to originate purely from the spin of the electron. Consequently, the total magnetic moment on each TM atom is  $N \times 1 \mu_B$ , where  $N$  is the total number of unpaired electrons in the  $3d$  shell of each TM atom.

The basic ionic theory suggests 4+ oxidation state of Cr and Mn cations in our monolayers, since C atom receives 4 electrons to reach stable octet configuration. Furthermore,  $\text{Cr}^{4+}$  ion has 20 electrons and the  $1s^2 2s^2 2p^6 3s^2 3p^6 3d^2$  electronic

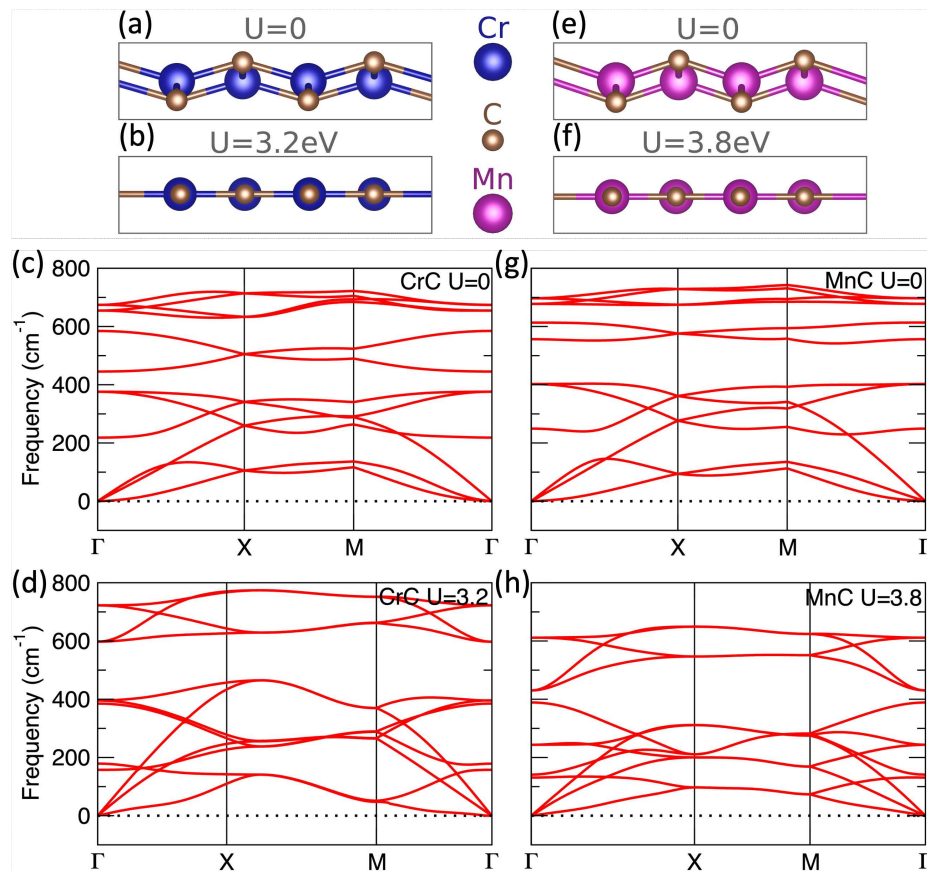


Figure 2: **Stability of CrC and MnC ferromagnetic monolayers.** The effect of Hubbard parameter  $U$  on monolayer structures of CrC (a and b) and MnC (e and f). The phonon dispersions of two materials for without  $U$  and optimal  $U$  shown in (c, d, g and h), proving dynamical stability of the shown structures.

configuration, while  $\text{Mn}^{4+}$  ion 21 electrons and the  $1s^2 2s^2 2p^6 3s^2 3p^6 3d^3$  electronic configuration. This means that one expects  $2 \mu_B$  per Cr atom and  $4 \mu_B$  per primitive unit cell in CrC, and  $3 \mu_B$  per Mn atom and  $6 \mu_B$  per primitive unit cell in MnC. Ionic theory predicts no moment per C atom in either cases, due to the mentioned stable octet configuration.

For a more precise account of magnetic moments per atom we resort to DFT calculations, and find that: (1) in case of CrC, the magnetization per Cr atom is  $2.85 \mu_B$  and per C atom  $-0.72 \mu_B$ , resulting in  $4.27 \mu_B$  per primitive unit cell; (2) in case of MnC, the magnetization per Mn atom is  $3.88 \mu_B$  and per C atom  $-0.77 \mu_B$ , resulting in  $6.22 \mu_B$  per primitive unit cell. The DFT results do corroborate the crude ionic theory regarding the total magnetization of the unit cell, but also reveal the significant hybridization between ( $d$ ) orbitals of TM atoms and ( $p$ ) orbitals of C atoms - causing a rather significant magnetization on otherwise non-magnetic C atoms.

The origin of the magnetic moments on all atoms involved is discussed in detail in the chapter “MAGNETIC MOMENTS” in the † Supplementary Information. Next to

it, we comment on rather large discrepancy between ionic and DFT predictions of the magnetic moments on both TM and C atoms.

However, in order for a system to host measurable magnetic order, next to the non-zero magnetic moments on TM ions, it must also host significant interaction between them. Unlike the initial estimates using the method based on mapping between total energies of the DFT and the Heisenberg Hamiltonians, we now calculate the magnetic exchange by mapping the energy variations due to the infinitesimal rotation of the magnetic moment on TM atoms from the reference FM state, between the DFT Hamiltonian in the localized-orbital basis set, and the Heisenberg Hamiltonian  $H = \sum_{\langle i,j \rangle} \mathbf{S}_i \mathbf{J}_{i,j} \mathbf{S}_j$ , as implemented in the TB2J code [38]. In the latter Hamiltonian,  $\mathbf{S}_i$  denotes the unit 3D vector of the magnetic moment on the  $i^{\text{th}}$  TM atom;  $3 \times 3$  matrix  $\mathbf{J}_{i,j}$  stands for interaction between magnetic moments on  $i$ -th and  $j$ -th TM atoms; and  $\langle i,j \rangle$  denotes  $i \neq j$ , with avoided double counting. The SIA matrix cannot be calculated using this formalism (for details see [38]), therefore it is not explicitly written in the used Heisenberg Hamiltonian. However, SIA is not negligible, and correspondingly must be taken into account during e.g. the calculation of  $T_c$  for the FM order. Therefore, we combine SIA reported in Table 1, together with the  $\mathbf{J}_{i,j}$  calculated using TB2J to construct the total model Hamiltonian for eventual  $2^{\text{nd}}$ -principles calculations:

$$H = \sum_{\langle i,j \rangle} \mathbf{S}_i \mathbf{J}_{i,j} \mathbf{S}_j + \sum_i \mathbf{S}_i \mathbf{A}_{i,i} \mathbf{S}_i. \quad (1)$$

The main advantage of TB2J and the Green's-function-based methodology over the total energy mapping is the ability to orbitally disentangle the origins of magnetic interactions [39], and also the ability to calculate interactions between *all* different neighbors within a large supercell upon a *single* DFT calculation on the primitive unit cell. In particular, we have calculated the matrices  $\mathbf{J}_{i,j}$  up to the  $284^{\text{th}}$  NN for both materials.

Our results obtained using TB2J obey the symmetry-imposed constraints - i.e. all off-diagonal elements of all  $\mathbf{J}_{i,j}$  matrices are exactly 0. The diagonal part of each matrix can further be split - as presented in Table 1 - into the isotropic ( $J_{i,j} = J_{i,j}^{xx} = J_{i,j}^{yy}$ ) and the anisotropic part ( $\Delta = J_{i,j}^{zz} - J_{i,j}^{xx}$ ). The anisotropic part of the exchange,  $\Delta$ , in either system does not exceed few (1-6)  $\mu\text{eV}$ , and is comparable with the rounding error in our calculations. Therefore, we consider  $\Delta$  as effectively 0, and we subscribe the stabilization of the magnetic order in these 2D materials to just  $J_{i,j}$  and SIA §.

In Fig. 3 we present our TB2J results for  $J_{i,j}$  up to the  $6^{\text{th}}$  NN. One notices in Fig. 3 that  $1^{\text{st}}$  and  $2^{\text{nd}}$  NN interactions are strong (few tens of meV), an order of magnitude larger compared to usually encountered isotropic exchange values (few meV) in 2D materials. Another observation is that even pairs over 1 nm distance have small but non-zero exchange interaction, of few hundreds of  $\mu\text{eV}$ . However, since these are much smaller than the  $1^{\text{st}}$  and  $2^{\text{nd}}$  NN interactions, in what follows, we

§ This is in qualitative agreement with results reported in Table 1, where  $\Delta$  was found to be much smaller than SIA and  $J_{i,j}$ .



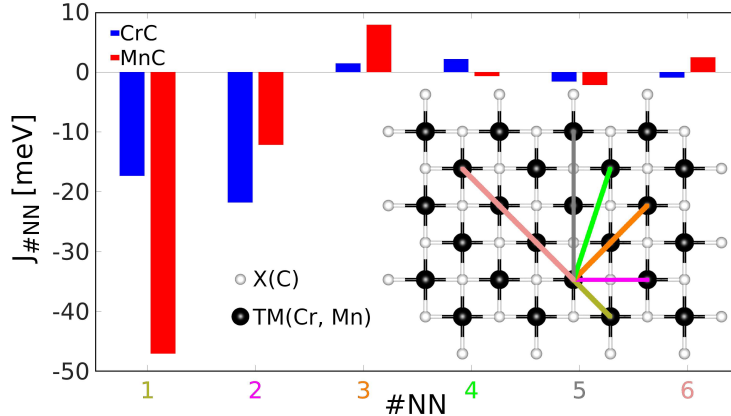


Figure 3: **The isotropic magnetic exchange, per neighboring pair.** The isotropic exchange interactions in CrC (blue) and MnC (red), calculated using Green’s function method as implemented in TB2J. The inset depicts the numerical labeling of the nearest-neighbor sites within the structure.

focus on the first two NN pairs with giant  $J_{i,j}$ , being essential for the high- $T_C$  GKA ferromagnetism. We use exchange interaction parameters calculated with TB2J, and SIA from Table 1 to build the Heisenberg Hamiltonian as explained above, to then employ Monte Carlo simulations to evaluate the stability of the FM order with respect to temperature. In Fig. 4, we present the thereby obtained evolution of (normalized) magnetization ( $M_{st}/M_s$ ), magnetic susceptibility ( $\chi$ ), and specific heat ( $C_v$ ), as a function of temperature. One clearly sees that estimated critical temperatures of the FM order in both CrC and MnC *exceed the room temperature*, being 307 K and 428 K respectively. Even though anisotropy is in general required to stabilize magnetic order in 2D above 0 K - in our case that is SIA - the main reason for such a large  $T_C$  lies in the particularly large isotropic exchange between the 1<sup>st</sup> as well as the 2<sup>nd</sup> NN pairs of TM atoms. Table 1 provides Curie and Neel temperature values for *t*-TMX structures. Notably, VN, CoN, and NiTe structures exhibit ferromagnetic properties; however, their respective Curie temperatures are significantly lower compared to those of CrC and MnC. This phenomenon can be primarily attributed to two key factors: weakened exchange interactions and strong Single Ion Anisotropy (SIA). This weakened exchange interaction and strong SIA inherently limits their ability to maintain ferromagnetic order at elevated temperatures, thus resulting in lower Curie temperatures when contrasted with CrC and MnC. Conversely, antiferromagnetic materials exhibit Neel temperatures in proximity to absolute zero (0 K) due to the significant impact of SIA. This low Neel temperature signifies the point at which antiferromagnetic materials undergo a transition to a non-magnetic state. The details about calculations of Curie and Neel temperatures can be found in † Supplementary Information.

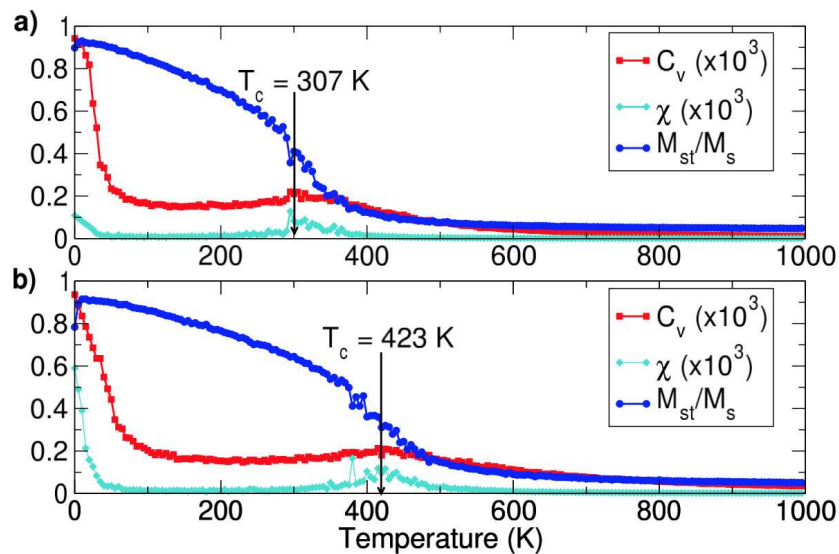


Figure 4: **Thermal stability of the long-range magnetic order.** Magnetization, specific heat and magnetic susceptibility of (a) CrC and (b) MnC, as a function of temperature. In graphs, the units of the specific heat is dimensionless, and magnetic susceptibility is in  $\mu_B^2/\text{Ha}$ .

### 3. Discussion

Having presented the core results, we next detail the origin of the magnetic interactions behind the observed high Curie temperature in monolayer *t*TMXs, bearing in mind the original assumptions following from the GKA rules. To shed the light on the source of the large exchange  $J_{i,j}$ , we look into the orbitally-resolved contributions.

Our initial assumption was that the gross of the exchange interactions originates from the exchange between the *d* orbitals of the interacting TM atoms (*d-d* exchange). In order to properly describe the physics behind our observations, we treat *3s*, *3p*, *3d*, *4s*, and *4p* as valence orbitals on TM atoms. Further, we quantify the contributions of each orbital-to-orbital interaction between the neighboring TM atoms (e.g. *4s* on TM1 and *3d* on TM2), to the total exchange between them. For facilitated interpretation, we consider the contributed interactions between each type of orbital on TM1 ( $a = 3s, 4s, 3p, 3d,$  and  $4p$ ) and only *3d* orbitals on TM2 ( $b = 3d$ ), for the first three NN magnetic interactions  $J_{\#NN}^{a,b}$ , as shown in Fig. 5. It is rather obvious from Fig. 5 that TM1(*3d*)-TM2(*3d*) interactions dominate (being several tens of meV strong), and determine the magnetic order in the system - in this case the FM one. Interactions between other types of orbitals on one TM and *3d* orbitals on the other are generally at least an order of magnitude smaller. Therefore, after *d-d* exchange is proven to be crucial for the large exchange and room-temperature magnetism in *t*TMXs, we next decompose it into the exchanges between individual *d*-orbitals of the interacting pair of TM atoms, to disentangle the key contributors. The results per *d*-orbital and per material are shown in Fig. 6.

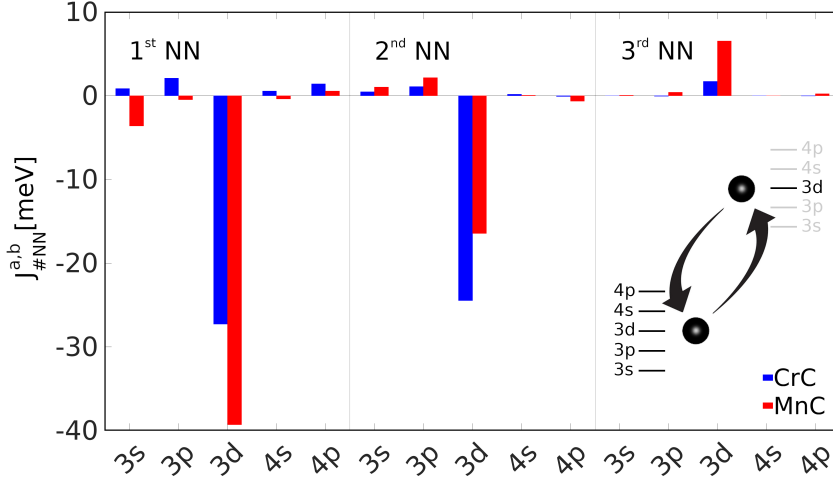


Figure 5: **Orbitally-decomposed magnetic interactions.** The magnetic exchange interactions in CrC and MnC, for the three nearest-neighbor pairs. As illustrated in the inset, for every pair the contributions are discerned per orbital  $a$  of TM1 ( $a = 3s, 4s, 3p, 3d, 4p$ ), each interacting with just one orbital ( $b = 3d$ ) of TM2.

### 3.1. The nearest-neighbor interaction

Owing to the square lattice symmetry of these monolayers, our original premise holds, and the empirical GKA rules are validated in the case of the 1<sup>st</sup> NN exchange - the ideally 90° TM-X-TM bond arrangement fosters a particularly strong FM interaction, stemming mainly from the  $d$ - $d$  exchange.

As seen in Fig. 6, the largest contribution to the 1<sup>st</sup> NN magnetic interaction in both considered materials comes from the interaction between  $d_{xz}$  on one TM atom, and  $d_{yz}$  on the other, together with its symmetric twin - TM1( $d_{yz}$ )-TM2( $d_{xz}$ ). We prescribe this exactly to the square-lattice geometry of the structure and the fact that the dumbbells of the  $d_{xz}$  on TM1 and  $d_{yz}$  on TM2 point along the bonds to the (X1) ligand atom between them in the structure (analogously for  $d_{yz}$  on TM1 and  $d_{xz}$  on TM2, interacting via the adjacent ligand X2). Moreover, after having a closer look at the DFT Hamiltonian in the localized basis set, we noticed that both  $d_{xz}$  on TM1 and  $d_{yz}$  on TM2 interact only with  $p_z$  on X1, while the other hopping matrix elements (with  $p_x$  and  $p_y$  on X1, and  $p_x$ ,  $p_y$ , and  $p_z$  on X2) are 0, because of the symmetry of the system. However, despite the fact that only three types of orbitals are involved -  $d_{xz}$ ,  $d_{yz}$ , and  $p_z$ , two contributions to the first-nearest-neighbor magnetic exchange from this class differ in both sign and size - TM1( $d_{xz}$ )-TM2( $d_{xz}$ ) and TM1( $d_{yz}$ )-TM2( $d_{yz}$ ) are weak AFM, while TM1( $d_{xz}$ )-TM2( $d_{yz}$ ) and TM1( $d_{yz}$ )-TM2( $d_{xz}$ ) are strong FM. In case of the second-nearest-neighbor sign is the same, but magnitude is still drastically different. The same ingredients but different outcome suggest fundamental difference in physical processes leading to these two contributions. After detailed examination of Hamiltonian and additional analysis performed, we have clearly established that indirect



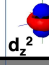

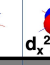


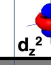
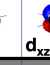

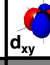

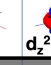





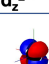
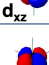
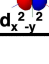
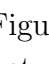
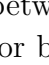


	CrC	MnC	Orbitally Decomposed Interactions														
	1 <sup>st</sup> NN					2 <sup>nd</sup> NN					3 <sup>rd</sup> NN						
																	
	15.02	0	-4.10	0	0	2.41	0	0	0	0	-0.97	0	0.11	0	0		
	-17.47	0	0.23	0	0.006	-3.28	0	0	0	0	8.19	0	-0.16	0	0		
	0	4.84	0	-22.44	0	0	-4.40	0	0	0	0	-0.63	0	2.11	0		
	0	0.45	0	-15.14	0	0	-0.04	0	0	0	0	0.31	0	-1.17	0		
	-4.10	0	1.78	0	0	0	0	-0.01	-0.002	-1.11	0.11	0	-0.02	0	0		
	0.23	0	0.37	0	0	0	0	0.10	0	-1.11	-0.16	0	-0.02	0	0		
	0	-22.44	0	4.58	0	0	0	-0.002	-18.98	0	0	2.11	0	-0.65	0		
	0	-15.14	0	0.56	0	0	0	0	-9.70	0	0	-1.17	0	0.33	0		
	0	0	0	0	-0.44	0	0	-1.11	0	-1.26	0	0	0	0	-0.46		
	0.006	0	0	0	6.60	0	0	-1.11	0	1.33	0	0	0	0	0.36		

Figure 6: **Sub-orbitally-decomposed 3d-3d interactions.** The magnetic exchange between five different 3d ( $d_{xy}$ ,  $d_{yz}$ ,  $d_{z^2}$ ,  $d_{xz}$  and  $d_{x^2-y^2}$ ) orbitals on first three NN pairs, for both CrC and MnC monolayers. CrC and MnC are indicated using dark and light shading, respectively.

interaction of  $d_{xz}$ - $d_{xz}$  and  $d_{yz}$ - $d_{yz}$  involves two  $p_z$  of two C atoms (“N” superexchange in case of the 90 degrees first-nearest-neighbor), while indirect interaction of  $d_{xz}$ - $d_{yz}$  and  $d_{yz}$ - $d_{xz}$  involves only one  $p_z$  of single C atom (“L” superexchange for the 90 degrees first-nearest-neighbor and “—” superexchange for the 180 degrees second-nearest-neighbor), and that this is the sole difference between two processes. In addition, we established that dominant second-nearest-neighbor term originates from the same type of single-p-mediated superexchange. To summarize: single-p-mediated superexchange leads to giant FM orbitally-resolved contributions to the magnetic exchange, which in turn lead to large total magnetic exchange between TM atoms, which in turn allows long-range FM order to maintain even at the room temperature. For details, we refer interested reader to the † Supplementary Information.

Another significant contribution to the total exchange between the 1<sup>st</sup> NN pair originates from TM1( $d_{xy}$ )-TM2( $d_{xy}$ ) interactions. In that case, the  $d_{xy}$  orbitals on TM1 and TM2 point towards each other directly and have significant direct overlap, however, there is also significant hopping between  $d_{xy}$  on both TM1 and TM2 and  $p_x$  and  $p_y$  orbitals on both nearest X atoms (X1 and X2). This increased complexity of the physical picture causes differences in the sign and the strength of those particular contributions in the two considered compounds: in case of CrC this contribution is AFM, while in case of MnC it is FM. The main reason for the difference in this orbital contribution lies in the different *atomic environment* - the ordering and occupation of the atomic  $d(p)$  orbitals on TM(X) atoms - and different behavior of direct exchange in the particular environment. In case of the atomic environment in CrC, the superexchange solely determines the orbital contribution to the total magnetic exchange and it is AFM,

while in case of MnC, direct- and superexchange compete in such atomic environment that the result is the FM coupling. Details of these findings are made available in the † Supplementary Information.

Both compounds host several other non-zero interactions between different  $d$  orbitals, e.g.  $d_{xy}$  on TM1 and  $d_{z^2}$  on TM2. Even though these terms are much smaller than the dominating ones discussed above, they are still sizable (several meV) and they do affect the total exchange, albeit on tertiary level. In particular TM1( $d_{xy}$ )-TM2( $d_{z^2}$ ) contribution is very sensitive to the alteration of the superexchange hopping TM( $d_{xy}$ )-X( $p_{x/y}$ ), hence we note that superexchange mechanism plays an important role here. For more discussion on their origin and behavior, we refer the reader to the † Supplementary Information.

### 3.2. The next-nearest and further-neighbor interactions

Although our initial premise of strong FM interactions between the first nearest neighbors was validated, we point out at this stage that plain GKA rules are not sufficient to interpret the magnetic behavior of a 2D material, even in the case of an ideally planar square-lattice structure. Namely, the 2<sup>nd</sup> NN interaction is expected to be AFM according to the GKA rules, due to the 180° TM-X-TM bond alignment - but we have observed the (strong) opposite in both materials of interest.

In what follows, we present the results for the TM1-X-TM2 bonds being aligned with the global  $x$  coordinate (as the case of TM1-X-TM2 along  $y$  is completely analogous). As was the case with the 1<sup>st</sup> NN interaction, the orbitals aligned with the direction of TM-X-TM bonds are mainly responsible for the large total exchange of the 2<sup>nd</sup> NN pair as well - i.e. TM1( $d_{xz}$ )-TM2( $d_{xz}$ ) interaction is the dominant one in this case. The dumbbells of these two  $d$  orbitals both point towards the common X atom, and only interact with its  $p_z$  orbital.

The fact that the dominating contributions to the 1<sup>st</sup> and 2<sup>nd</sup> NN interactions are originating from the same physical process - i.e. from two  $d$  orbitals on two TM atoms that are oriented towards the common ligand atom, and interact only with its  $p_z$  orbital - leads towards the conclusion that they should be of the same sign and comparable strength, as they indeed are in our results (strongly FM). That said, the GKA rules assume the dominant contribution to the AFM superexchange in case of 180° TM-X-TM bonds to be via the  $p$  orbital of X, whose dumbbell is aligned with TM-X-TM direction [40, 30] - which would be the  $p_x$  orbital in the above discussion. However, even though we find these contributions to be AFM as GKA rules would suggest, we also find that they are an order of magnitude smaller than the dominant contributions, involving the  $p_z$  orbital. Therefore, the disagreement between our results and GKA rules originates in the fact that mechanism considered dominant by GKA (superexchange involving the  $p_x$ , or  $p_\sigma$ ) is secondary in our case, and vice versa - the mechanism considered secondary by GKA (superexchange involving the  $p_z$ , or  $p_\pi$ ) appears to be dominant in the two materials of our interest. For interested readers, this is discussed in more detail within

the † Supplementary Information.

In case of the 3<sup>rd</sup> NN exchange, the geometry is very similar to the 1<sup>st</sup> NN exchange, hence one expects to have the same dominant contributions. We find that the three main contributions in both materials are indeed the same ones as in the case of the 1<sup>st</sup> NN, i.e.  $d_{xz}$ - $d_{yz}$ ,  $d_{yz}$ - $d_{xz}$ , and  $d_{xy}$ - $d_{xy}$ . However, their observed behavior is more complicated. In case of CrC the TM1( $d_{xz}$ )-TM2( $d_{yz}$ ) and TM1( $d_{yz}$ )-TM2( $d_{xz}$ ) are contributing the most, however to AFM order (positive exchange parameter), while the second largest contribution comes from TM1( $d_{xy}$ )-TM2( $d_{xy}$ ) and it is FM. In case of MnC the main contribution comes from TM1( $d_{xy}$ )-TM2( $d_{xy}$ ) and it is AFM. The interaction between TM1( $d_{xz}$ )-TM2( $d_{yz}$ ) and TM1( $d_{yz}$ )-TM2( $d_{xz}$ ) is again FM, however their magnitude affects the total 3<sup>rd</sup> NN exchange significantly less. Since the 3<sup>rd</sup> NN exchange is negligible compared to the 1<sup>st</sup> and 2<sup>nd</sup> NN exchange, we will not detail these interactions. We see however that sign and strength of the orbital contributions to the 3<sup>rd</sup> NN exchange are mainly determined by the orbital ordering and occupation of Cr and Mn atoms - i.e. their atomic environment - and the fact that in different environment, the different mechanisms may be dominating. In case of the TM1( $d_{xy}$ )-TM2( $d_{xy}$ ) contribution, our results suggest that in case of CrC there is the competition between direct and superexchange, while in MnC it is the usual superexchange through the X ligand that dominates. By comparing the results for the first- and the third-nearest-neighbor exchange in two materials, one could argue that in case that atomic environment stimulates the superexchange alone, the result will be AFM interaction (the first-nearest-neighbor in CrC, and third-nearest-neighbor in MnC). On the other hand, when atomic environment stimulates the competition between different exchange mechanisms (the first-nearest-neighbor in MnC, and third-nearest-neighbor in CrC) resulting interaction between TM1( $d_{xy}$ )-TM2( $d_{xy}$ ) will be FM. For interested readers, we provide brief additional discussion of the effect of atomic environment to the third-nearest-neighbor magnetic exchange in the † Supplementary Information.

#### 4. Conclusions

In summary, after a computational throughput screening of the whole family of *t*TMX materials, we have identified two dynamically stable and ideally 2D flat Lieb-like magnetic crystals, CrC and MnC. According to the seminal Goodenough-Kanamori-Anderson rules, materials of such symmetry are prone to host pronouncedly high ferromagnetic exchange interaction. Our detailed analysis of the magnetic properties has shown that both Cr and Mn ions indeed have sizable magnetic moments, that materials host large isotropic magnetic interactions (order of 10 meV), that exchange anisotropy is negligible in these systems (order of 1  $\mu$ eV), and that stabilization of the long-range magnetic order in these materials should be prescribed to single-ion anisotropy (order of 0.1 meV). As a result of this large isotropic exchange and non-zero single-ion anisotropy, the Curie temperature for ferromagnetic transition of these materials exceeds the room temperature - 307 K in CrC and 428 K in MnC.

In detailed analysis presented, we pinpoint the sole physical mechanism that lies in the origin of room temperature magnetism in these systems - geometry-selected single-*p*-mediated superexchange. We indisputably show that this mechanism leads to the large FM contributions for both the first- and the second-nearest-neighbor magnetic exchange between TM atoms, in both CrC and MnC.

In case of the 3<sup>rd</sup> NN, which was of secondary importance in our systems, we could not establish a criterion for single dominant contribution based on geometry, however, even there two contributions were identified as leading ones. Finally we have shown that interactions beyond the 3<sup>rd</sup> NN are far smaller and may be neglected in any prediction of experimentally measurable physical properties of these systems.

In conclusion, we outline the key general rules for room temperature magnetism in this material family:

(i) Matrix elements in TB-like Hamiltonian associated with direct d-d orbital interaction must be *negligible* - at least  $\sim 5$ -10 times smaller than matrix elements connected with the indirect interaction.

(ii) The superexchange process should be mediated only with the single *p* orbital of single non-magnetic atom - “L” superexchange in case of the first-nearest-neighbor and “—” superexchange in case of the second-nearest-neighbor. This is guaranteed in the flat square-lattice.

(iii) Magnetic atoms should be chosen from the first half of the first row of transition metals (V, Cr, Mn, Fe) in order to guarantee “small” number of d-electrons ( $\leq 5$ ), which will ensure the high-spin state. Other typical magnetic elements (Co, Ni, Cu) may host low-spin state and therefore not comply with our conclusions.

Consequently, in any such system with sufficient anisotropy in magnetic interactions, the latter features will foster the large isotropic exchange and high critical temperature of the long-range magnetic order in two dimensions.

## 5. Acknowledgement

This work was supported by the Research Foundation-Flanders (FWO) and the Technological Research Council of Turkey (TUBITAK) under Contract No. 118F512. D.Š. is a doctoral fellow of FWO under Contract No. 11J4322N. The computational resources and services for this work were provided by the VSC (Flemish Supercomputer Center), funded by the FWO and the Flemish Government – department EWI.

## References

- [1] Huang B, Clark G and Navarro-Moratalla E e a 2017 *Nature* **546** 270–273 URL <https://doi.org/10.1038/nature22391>
- [2] Gong C, Li L and Li Z e a 2017 *Nature* **546** 265–269 URL <https://doi.org/10.1038/nature22060>
- [3] Xing W, Chen Y, Odenthal P M, Zhang X, Yuan W, Su T, Song Q, Wang T, Zhong J, Jia S,

- Xie X C, Li Y and Han W 2017 *2D Materials* **4** 024009 URL <https://doi.org/10.1088/2053-1583/aa7034>
- [4] Lado J L and Fernández-Rossier J 2017 *2D Materials* **4** 035002 URL <https://doi.org/10.1088/2053-1583/aa75ed>
- [5] Webster L and Yan J A 2018 *Phys. Rev. B* **98**(14) 144411 URL <https://link.aps.org/doi/10.1103/PhysRevB.98.144411>
- [6] Xu C, Feng J and Xiang H e a 2018 *npj Comput Mater* **4**(57) URL <https://doi.org/10.1038/s41524-018-0115-6>
- [7] Kashin I V, Mazurenko V V, Katsnelson M I and Rudenko A N 2020 *2D Materials* **7** 025036 URL <https://doi.org/10.1088/2053-1583/ab72d8>
- [8] Deng Y, Yu Y and Song Y e a 2018 *Nature* **563** 94–99 URL <https://doi.org/10.1038/s41586-018-0626-9>
- [9] Jiang S, Li L and Wang Z e a 2018 *Nature Nanotech* **13** 549–553 URL <https://doi.org/10.1038/s41565-018-0135-x>
- [10] Huang B, Clark G and Klein D e a 2018 *Nature Nanotech* **13** 544–548 URL <https://doi.org/10.1038/s41565-018-0121-3>
- [11] Bonilla M, Kolekar S and Ma Y e a 2018 *Nature Nanotech* **13** 289–293 URL <https://doi.org/10.1038/s41565-018-0063-9>
- [12] Roemer R, Liu C and Zou K 2020 *npj 2D Mater Appl* **4** 33 URL <https://doi.org/10.1038/s41586-021-04337-x>
- [13] Song Q, Occhialini C and Ergeçen E e a 2022 *Nature* **602** 601–605 URL <https://doi.org/10.1038/s41586-021-04337-x>
- [14] Mermin N D and Wagner H 1966 *Phys. Rev. Lett.* **17**(22) 1133–1136 URL <https://link.aps.org/doi/10.1103/PhysRevLett.17.1133>
- [15] Fei Z, Huang B and Malinowski P e a 2018 *Nature Materials* **17** 778–782 URL <https://doi.org/10.1038/s41563-018-0149-7>
- [16] Meng L, Zhou Z and Xu M e a 2021 *Nature Communications* **12** 809 URL <https://doi.org/10.1038/s41467-021-21072-z>
- [17] Ghosh A, Palit M, Maity S, Dwij V, Rana S and Datta S 2021 *Phys. Rev. B* **103**(6) 064431 URL <https://link.aps.org/doi/10.1103/PhysRevB.103.064431>
- [18] Zhang G, Guo F, Wu H, Wen X, Yang L, Jin W, Zhang W and Chang H 2022 *Nature Communications* **13**(1) 5067 URL <https://doi.org/10.1038/s41467-022-32605-5>
- [19] Wu H, Zhang W, Yang L, Wang J, Li J, Li L, Gao Y, Zhang L, Du J, Shu H and Chang H 2021 *Nature Communications* **12**(1) 5688 URL <https://doi.org/10.1038/s41467-021-26009-0>
- [20] O'Hara D J, Zhu T, Trout A H, Ahmed A S, Luo Y K, Lee C H, Brenner M R, Rajan S, Gupta J A, McComb D W and Kawakami R K 2018 *Nano Letters* **18** 3125–3131 pMID: 29608316 URL <https://doi.org/10.1021/acs.nanolett.8b00683>
- [21] Kan M, Adhikari S and Sun Q 2014 *Phys. Chem. Chem. Phys.* **16**(10) 4990–4994 URL <http://dx.doi.org/10.1039/C3CP55146F>
- [22] Boukhvalov D W and Politano A 2020 *Nanoscale* **12**(40) 20875–20882 URL <http://dx.doi.org/10.1039/D0NR04663A>
- [23] Chua R, Zhou J, Yu X, Yu W, Gou J, Zhu R, Zhang L, Liu M, Breese M B H, Chen W, Loh K P, Feng Y P, Yang M, Huang Y L and Wee A T S 2021 *Advanced Materials* **33** 2103360 (*Preprint* <https://onlinelibrary.wiley.com/doi/pdf/10.1002/adma.202103360>) URL <https://onlinelibrary.wiley.com/doi/abs/10.1002/adma.202103360>
- [24] Sun Y, Zhuo Z, Wu X and Yang J 2017 *Nano Lett.* **17**(5) 2771–2777 URL <https://doi.org/10.1021/acs.nanolett.6b04884>
- [25] Jiang Z, Wang P, Xing J, Jiang X and Zhao J 2018 *ACS Appl. Mater. Interfaces* **10**(45) 39032–39039 URL <https://doi.org/10.1021/acsami.8b14037>
- [26] Zhang C, Nie Y, Sanvito S and Du A 2019 *Nano Lett.* **19**(2) 1366–1370 URL <https://doi.org/10.1021/acs.nanolett.8b05050>
- [27] Liu L, Chen S, Lin Z and Zhang X 2020 *J. Phys. Chem. Lett.* **11**(18) 7893–7900 URL <https://doi.org/10.1021/acs.nanolett.8b05050>



- [//doi.org/10.1021/acs.jpcllett.0c01911](https://doi.org/10.1021/acs.jpcllett.0c01911)
- [28] Wu D, Zhuo Z, Lv H and Wu X 2021 *J. Phys. Chem. Lett.* **12**(11) 2905–2911 URL <https://doi.org/10.1021/acs.jpcllett.1c00454>
- [29] Goodenough J B 1955 *Phys. Rev.* **100**(2) 564–573 URL <https://link.aps.org/doi/10.1103/PhysRev.100.564>
- [30] Kanamori J 1959 *Journal of Physics and Chemistry of Solids* **10** 87–98 ISSN 0022-3697 URL <https://www.sciencedirect.com/science/article/pii/0022369759900617>
- [31] Anderson P W 1959 *Phys. Rev.* **115**(1) 2–13 URL <https://link.aps.org/doi/10.1103/PhysRev.115.2>
- [32] Anderson P W 1963 *Theory of Magnetic Exchange Interactions: Exchange in Insulators and Semiconductors (Solid State Physics vol 14)* (Academic Press) URL <https://www.sciencedirect.com/science/article/pii/S008119470860260X>
- [33] Gao L, Zhang Y F and Du S 2021 *Nano Research* **14** 2826–2830 URL <https://doi.org/10.1007/s12274-021-3294-2>
- [34] Kang L, Ye C, Zhao X, Zhou X, Hu J, Li Q, Liu D, Das C M, Yang J, Hu D, Chen J, Cao X, Zhang Y, Xu M, Di J, Tian D, Song P, Kutty G, Zeng Q, Fu Q, Deng Y, Zhou J, Ariando A, Miao F, Hong G, Huang Y, Pennycook S J, Yong K T, Ji W, Renshaw Wang X and Liu Z 2020 *Nature Communications* **11**(1) 3729 URL <https://doi.org/10.1038/s41467-020-17253-x>
- [35] Ong S P 2021 *Materials Project Documentation* URL <https://docs.materialsproject.org/methodology/materials-methodology/calculation-details/gga+u-calculations#u-values>
- [36] Šabani D, Bacaksiz C and Milošević M V 2020 *Phys. Rev. B* **102**(1) 014457 URL <https://link.aps.org/doi/10.1103/PhysRevB.102.014457>
- [37] Timrov I, Marzari N and Cococcioni M 2022 *Computer Physics Communications* **279** 108455 ISSN 0010-4655 URL <https://www.sciencedirect.com/science/article/pii/S0010465522001746>
- [38] He X, Helbig N, Verstraete M J and Bousquet E 2021 *Computer Physics Communications* **264** 107938 ISSN 0010-4655 URL <https://www.sciencedirect.com/science/article/pii/S0010465521000679>
- [39] Kashin I V e a 2020 *2D Materials* **7** 025036 URL <https://iopscience.iop.org/article/10.1088/2053-1583/ab72d8>
- [40] van Vleck J H 1951 *J. Phys. Radium* 262–274 URL <https://doi.org/10.1051/jphysrad:01951001203026200>

† Supplementary Information (SI) available: [details of any supplementary information available should be included here]. See DOI: 10.1039/cXCP00000x/